Title
A Molecular Switch for the Orientation of Epithelial Cell Polarization

Journal
Developmental Cell, 31(2)

ISSN
1534-5807

Authors
Bryant, David M
Roignot, Julie
Datta, Anirban
et al.

Publication Date
2014-10-01

DOI
10.1016/j.devcel.2014.08.027

Peer reviewed

Published in final edited form as:
Dev Cell. 2014 October 27; 31(2): 171–187. doi:10.1016/j.devcel.2014.08.027.

A Molecular Switch for the Orientation of Epithelial Cell Polarization

David M. Bryant[1,3], **Julie Roignot**[1], **Anirban Datta**[1], **Arend W. Overeem**[1], **Minji Kim**[1], **Wei Yu**[1], **Xiao Peng**[1], **Dennis J. Eastburn**[1], **Andrew J. Ewald**[1,4], **Zena Werb**[1], and **Keith E. Mostov**[1,2,*]

[1]Department of Anatomy, University of California, San Francisco, San Francisco, CA 94158-2140, USA

[2]Department of Biochemistry and Biophysics, University of California, San Francisco, San Francisco, CA 94158-2140, USA

SUMMARY

The formation of epithelial tissues containing lumens requires not only the apical-basolateral polarization of cells, but also the coordinated orientation of this polarity such that the apical surfaces of neighboring cells all point toward the central lumen. Defects in extracellular matrix (ECM) signaling lead to inverted polarity so that the apical surfaces face the surrounding ECM. We report a molecular switch mechanism controlling polarity orientation. ECM signals through a β1-integrin/FAK/p190RhoGAP complex to down-regulate a RhoA/ROCK/Ezrin pathway at the ECM interface. PKCβII phosphorylates the apical identity-promoting Podocalyxin/NHERF1/Ezrin complex, removing Podocalyxin from the ECM-abutting cell surface and initiating its transcytosis to an apical membrane initiation site for lumen formation. Inhibition of this switch mechanism results in the retention of Podocalyxin at the ECM interface and the development instead of collective front-rear polarization and motility. Thus, ECM-derived signals control the morphogenesis of epithelial tissues by controlling the collective orientation of epithelial polarization.

INTRODUCTION

The most fundamental type of tissue is epithelium, where in the simplest case a monolayer of cells lines a cavity or surface. Epithelial cells have an apical (AP) plasma membrane (PM) facing the lumen or free surface, a lateral PM touching adjacent cells, and a basal PM contacting underlying extracellular matrix (ECM). The AP-basolateral (BL) polarity of each cell has a specific orientation, and this orientation is coordinated between cells to form the tissue (e.g., in a hollow tube the AP PMs of neighboring cells are radially polarized around a

*Correspondence: keith.mostov@ucsf.edu.
[3]Present address: CRUK Beatson Institute for Cancer Research, University of Glasgow, Glasgow G61 1BD, UK
[4]Present address: Department of Cell Biology, Center for Cell Dynamics, Johns Hopkins University, Baltimore, MD 21205, USA

SUPPLEMENTAL INFORMATION

Supplemental Information includes Supplemental Experimental Procedures, six figures, and three movies and can be found with this article online at http://dx.doi.org/10.1016/j.devcel.2014.08.027.

central lumen). How the polarity of cells is oriented is a fundamental, yet largely unanswered, question.

Interaction of cells with ECM and other cells provide spatial cues to localize the BL PM (Bryant and Mostov, 2008). During morphogenesis of hollow organs, a lumen surrounded by AP PM often forms de novo at the center of a solid mass of cells. As a model to study this, we use MDCK cells grown as hollow cysts in 3D gels of Matrigel, a type of ECM. When single MDCK cells are plated in Matrigel, some of their AP PM proteins, such as Podocalyxin/gp135 (Podxl), are found at the PM in contact with the ECM. After the first division, the doublets have two PM domains, a cell-cell contact and an ECM-abutting surface. The orientation of polarity at this stage is termed “inverted,” in that Podxl and some other AP PM proteins are found only at the peripheral, ECM-abutting PM. As the cyst develops, polarity reorients and these AP proteins relocalize, typically at the two-cell stage, to a centrally located patch of existing cell-cell contact, called the AP membrane initiation site (AMIS). The AMIS is converted into a nascent AP PM, containing Podxl and other AP proteins (Bryant et al., 2010; Ferrari et al., 2008), followed by its expansion to become a mature lumen. A similar process occurs in the developing mouse dorsal aorta, where Podxl is targeted to an AMIS-like patch and stabilized by the Ezrin-Radixin-Moesin (ERM) family protein Moesin, at cell-cell contacts to initiate de novo AP PM formation. This reorientation of polarity, which mirrors aspects of in vivo lumen formation, makes MDCK cystogenesis an appealingly simple system to study how the orientation of epithelial polarity is controlled.

MDCK cysts with loss of Rac1 function fail to reorient, so that cysts retain Podxl and other AP proteins at the ECM-abutting periphery and lumens fail to form (O’Brien et al., 2001). This was an early clue that establishment of epithelial polarity could be separated from orientation of polarity. Blockade of β1-integrin or perturbation of the Rac1 effector, Pak1, similarly prevents reorientation, leaving cysts in an inverted state (deLeon et al., 2012; Yu et al., 2005). Such abnormal inversion can be prevented by simultaneous RhoA-ROCKI pathway inhibition (Yu et al., 2008). In multiple intestinal atresia patients, mutation in tetratrico-peptide repeat domain-7A (TTC7A) similarly causes an inversion of enterocyte polarity; treatment with a ROCK inhibitor rescues normal polarity orientation of enterocytes in 3D culture (Bigorgne et al., 2014). These data suggested that polarity reorientation is controlled by a pathway involving integrins, TTC7A, and the antagonism between the Rac1 and RhoA GTPases, although how these pathways interface to control orientation is largely unknown. In mammary epithelia in 3D, however, Rac1 appears to be dispensable, and an integrin-linked kinases (ILK)-microtubule pathway is instead utilized (Akhtar and Streuli, 2013). Cell- or tissue-type differences in polarization may therefore exist.

Work from many laboratories has analyzed how the AP PM is constructed de novo. Podxl and several other AP proteins are endocytosed from the ECM-abutting periphery and transcytosed to the AMIS. This vesicular transport pathway uses many components, including several Rab GTPases and their effectors, microtubules and the Cdc42/Par polarity complex (Akhtar and Streuli, 2013; Apodaca et al., 2012). Podxl is not only one of the earliest AP proteins delivered to the AMIS, but is also essential for building the AP PM and lumen (Datta et al., 2011; Strilić et al., 2009). The heavily glycosylated Podxl extracellular domain acts as an “anti-adhesin” (Strilić et al., 2010), inciting membrane repulsion between

neighboring cells, thereby generating the intracellular space that gives rise to the lumen. Neutralization of this electrostatic charge, or genetic deletion of Podxl, attenuates mouse aorta lumen formation (Strilić et al., 2009), Zebrafish pronephros development (Ichimura et al., 2013), and induces podocyte slit diaphragm effacement in vivo (Takeda et al., 2000; Takeda et al., 2001). Podxl null mice display profound kidney development defects and perinatal lethality (Doyonnas et al., 2001). Thus, the vectorial targeting and stabilization of Podxl at the AMIS is a crucial event in building a lumen-containing tissue.

These advances focus attention on the key question of how orientation is determined. Specifically, what controls the reorientation of polarity, so that Podxl and other AP PM proteins are removed from the peripheral PM and delivered to the AMIS to construct the AP PM and lumen de novo? Here, we elucidate the molecular mechanism that mediates the ECM-directed reorientation of polarity in the MDCK cyst model.

RESULTS

β1-Integrin Controls Apical Polarity Orientation by a RhoA-Suppressive Mechanism

To identify the ECM-derived signals that direct lumen formation, we examined β1-integrins. At the initially inverted, 2-cell stage, GFP-tagged (Figure 1A), or endogenous Podxl (Figure S1A available online) localized to the ECM-abutting periphery. In contrast, β1-integrin was not detected at the ECM interface, instead localizing to cell-cell contacts (Figure S1A, white arrowheads). As cysts developed, polarity reoriented. Podxl was internalized from the periphery and delivered to the nascent lumen. Concomitantly, β1-integrin now localized to the BL PM, with the active form of β1-integrin enriching at the ECM interface (Figures 1A and S1A, yellow arrowheads).

Inhibition of β1-integrin function with either blocking antibodies (Figures S1B and S1C, +AIIB2) or stable depletion (Figures 1B–1D and S1D–S1H) blocked the normal reorientation of polarity, so that inverted polarity persisted. Podxl was retained at the ECM-abutting periphery on part of a significant number of cysts (Figures 1B, yellow arrowheads, 1D, S1C, and S1G), although some rudimentary lumens formed. This retention of inversion was not complete, in that in a portion of the multicellular aggregates BL proteins localized at the ECM-abutting PM. Notably, β1-integrin inhibition did not induce complete absence of polarity in these multicellular structures, as indicated by the cortical asymmetry of Podxl and β-catenin (Figures 1B and S1D, arrows). This configuration has some features of the “front-rear” polarity of migrating neutrophils, with a pseudopod-like “front” and a uropod-like “rear” (Bryant and Mostov, 2008), although here this was on a multicellular scale. Note that even when β1-integrin was not perturbed, a small baseline of cysts (6% ± 2%) exhibited this front-rear polarity. Loss of β1-integrin function also perturbed normal cyst formation as indicated by decreased single lumen formation (SLF) (Figures 1C, S1B, and S1F). We therefore scored two types of polarity throughout this study: peripheral Podxl, indicating inverted or front-rear polarity; and SLF, indicating coordinated orientation of AP-BL polarity between neighboring cells to form a central lumen.

These phenotypes occurred with duplicate β1-integrin small hairpin RNAs (shRNAs) (Figures S1E–S1G) and were reversed by coexpression of RNAi-resistant β1-integrin-GFP

(Figures 1B–1D and S1H), which localized to BL membranes (Figures 1B and S1A). Conversely, overexpression of β1-integrin (wild-type [WT]) (Figures 1C, 1D, and S1H), or to a greater extent an autoclustered "active" mutant (V737N) (Paszek et al., 2005), increased rates of SLF, and reduced the baseline of front-rear polarized aggregates to below that in control cysts (Figures S1I–S1K). β1-integrin depletion also resulted in decreased expression of both α2- and α3-integrins (Figure S1E) and depletion of either α-integrin mirrored the perturbation of SLF and development of front-rear polarity seen upon β1-integrin depletion (Figures S1D–S1G). Thus β1-integrin, likely as α2β1 and α3β1 pairs, is not necessary for cell polarization per se, but instead controls the type of polarity, reorienting cells from initially inverted to lumen-containing cysts.

To determine whether the potential collective front-rear polarization we observed corresponded to migratory behaviors, we performed long-term time-lapse imaging of control and β1-integrin- inhibited cysts (Figure 1E; Movie S1). Time-lapse movies and tracing of cell/cyst outlines every 12 hr over 6 days revealed that initially both control and β1-integrin-inhibited (+AIIB2) cyst structures are motile (Figure 1E). Control cell aggregates quickly (≤39 hr after plating) lost such motility concomitant with morphogenesis to form spherical cysts (Movie S1, left), close to their initial observation site (Figure 1E, cyst trace). In contrast, β1-integrin-inhibited cysts migrated throughout the field of view, displaying long-range collective motility, often colliding to form large, irregularly shaped aggregates (Figure 1A; Movie S1, right). Compared to controls, a fan-shaped collective leading edge-like structure was often visible at the "front" of β1-integrin-perturbed cysts (Figure 1E, arrows), similar to the localization of Podxl in fixed images (Figure 1B, yellow arrowheads). These data suggest that β1-integrins are required to suppress long-range, potentially front-rear polarized collective motility.

β1-integrin inhibition (+AIIB2) markedly decreased activation of the β1-integrin effector FAK (Figure 1F, pY397). FAK depletion mimicked β1-integrin loss, decreasing SLF and markedly increasing the number of cysts with peripheral Podxl labeling (Figures 1G, arrows, 1H, and 1I). One function of β1-integrin in 3D culture is to suppress RhoA GTPase activation (Yu et al., 2008). Accordingly, inhibition of the RhoA effector kinases ROCKI/II (+Y-27632, 10 μM) in FAK-depleted cysts significantly rescued SLF and decreased the incidence of cysts with peripheral Podxl (Figures 1H and 1I). Thus, β1-integrin/FAK signaling controls AP-BL polarity by repressing RhoA-ROCK activation.

FAK controls fibroblast polarity by regulating formation of an adhesion complex containing the RhoA GAP p190A (Tomar et al., 2009); FAK-dependent p190A phosphorylation (pY1105) is required for p190A association with the complex. FAK depletion abolished p190A phosphorylation (pY1105; Figure S2A). Depletion of p190A significantly disrupted SLF and significantly increased the prevalence of cysts with peripheral Podxl, which could be robustly enhanced by coexpression of FAK phosphorylation-deficient, RNAi-resistant p190A (GFP-p190A Y1105F; Figures S2B–S2E). Together, these data indicate a β1-integrin/FAK/p190A module is required to switch the orientation of polarization from a largely inverted configuration to formation of a single lumen by repressing RhoA signaling.

RhoA-ROCKI-Ezrin Signaling Is Necessary and Sufficient for Collective Front-Rear Polarization

We next examined the necessity and sufficiency of RhoA-ROCKI for maintaining front-rear polarity and producing collective front-rear polarization. Corroborating our previous data (Yu et al., 2008), both RhoA and ROCKI were dispensable for SLF (Figures 2A and S2F–S2I), with robust depletion of ROCKI even slightly increasing SLF, similar to ROCK inhibition studies (Ferrari et al., 2008). In stark contrast, RhoA or ROCKI depletion significantly decreased the low baseline of front-rear polarization (Figures 2B, hash symbol, and S2I). Moreover, in β1-integrin-inhibited cysts, simultaneous RhoA depletion partially rescued SLF, attenuated front-rear polarization (Figures 2A–2C), and abolished the appearance of phase-dark ECM “tracks” that occurred near β1-integrin-inhibited cysts (Figures S2J and S2K, yellow arrowheads). The incomplete rescue of SLF may be due to lack of other β1-integrin effector pathway activation, such as Rac1-PAK1 (deLeon et al., 2012; Yu et al., 2005) or an ILK-microtubule pathway (Akhtar and Streuli, 2013). These data reveal a necessity for RhoA-ROCKI in front-rear, but not for AP-BL polarization.

β1-integrin inhibition in 3D cyst cultures causes a marked upregulation of global RhoA GTP loading (Yu et al., 2008). Coexpression of GFP-RhoA and a Cherry-tagged Rho-GTP-binding-domain (Cherry-RBD) construct to indicate RhoA-GTP localization (Murakoshi et al., 2011) revealed a sub-AP pool, below luminal Podxl labeling in control cysts (Figures 2D, control, white arrowheads, and 2E). In β1-integrin-inhibited cysts, GFP-RhoA instead localized to cell-cell contacts (Figure 2D, arrows) and intracellular compartments, but “active” RhoA only became apparent at the ECM interface, now coincident with Podxl labeling (Figures 2D, yellow arrowheads, and 2F). Combined GFP-RhoA overexpression/β1-integrin inhibition resulted in the complete inversion, rather than front-rear polarization of cysts, precluding detection of any potential front-rear RhoA-GTP gradient. Despite this, these data suggest that β1-integrins are necessary to suppress the inappropriate activation of RhoA at the ECM interface during AP-BL polarization.

To test the sufficiency of RhoA in promoting front-rear polarization, we examined cysts with Tetracycline-repressible (Tet-OFF) constitutively activate RhoA expression (myc-RhoA G14V) (Jou and Nelson, 1998). In the presence of the Tet analog Doxycycline (Figures 2G and 2H, +Dox) RhoA G41V was suppressed and luminal polarity formed with BL localization of the polarity protein Scribble (Figure 2G, arrow), and luminal localization of Podxl and the Podxl-interacting, RhoA-ROCK substrates, phosphorylated ERM proteins (Schmieder et al., 2004) (Figure 2G, pERM, white arrowheads). Induction of myc-RhoA G14V (Figure 2H; −DOX) strongly perturbed SLF (Figure 2I) and induced frank front-rear polarization, with AP Podxl at the front (arrowheads) and BL Scribble at the rear (Figures 2G, arrows, 2H, and 2J). Notably, RhoA activation resulted in a strong upregulation of pERM (Figure 2H, −Dox), which became preferentially apically enriched (Figure 2G, −Dox), although some pERM was detected at cell-cell contacts, likely representing ectopic, global RhoA activation. Similarly, perturbation of β1-integrin resulted in robust pERM upregulation (Figure 2K), which colocalized completely with Ezrin to the ECM-abutting periphery (Figure 2L, white arrows), instead of at the lumen in control cysts (yellow arrows). In contrast, we detected no specific AP or “front” enrichment of another major

RhoA-ROCK effector, the Myosin-2 light chain, which localized to all cortical domains of β1-integrin-inhibited cysts (Figure S2L). These data suggest that asymmetric activation and localization of Ezrin, downstream of RhoA-ROCKI, may control front-rear polarization.

To directly dissect this possibility, we stably depleted Ezrin in cells expressing an RNAi-resistant phosphomimetic ROCK-site mutant of Ezrin (Ezrin-GFP T567D). Compared to controls, phosphomimetic Ezrin, which was enriched at the "front" of cysts with Podxl (Figure 2M, box 1), although also localizing to a lesser degree at cell-cell contacts and the "rear" of cysts (Figure 2M, box 2), significantly lowered SLF (Figure 2N), and robustly induced front-rear polarization (Figures 2M and 2O). Taken together, these data indicate that RhoA-ROCK signaling promotes front-rear polarization by retaining Podxl localization at the ECM-abutting PM of part of aggregates.

The Podxl-NHERF1-Ezrin Complex Is Essential for AP-BL Polarization

Ezrin phosphorylation (pT567) releases autoinhibition, thereby activating Ezrin. NHERF-1/Ezrin-binding protein-50 (EBP50) is a dual PDZ domain-containing scaffold for numerous AP proteins (Fehon et al., 2010). Active Ezrin associates with and stabilizes the AP localization of a complex of Podxl and NHERF1, the latter two of which also directly interact through a PDZ-binding motif (PBM)-PDZ domain interaction (Fukasawa et al., 2011; Schmieder et al., 2004). RhoA-ROCK signaling may therefore stabilize the Podxl complex at the ECM-abutting PM by locally increasing the pool of active ERM proteins. We thus examined the dynamics of the Podxl-NHERF1-Ezrin complex during cystogenesis (12–24 hr). At the initially inverted, 2-cell stage Podxl localized to the ECM-abutting surface, where it colocalized strongly with NHERF1, pERM, and Ezrin (Figures 3A and S3A, white arrowheads; data not shown). During the internalization and transcytosis stages of lumenogenesis, NHERF1 and pERM no longer colocalized with Podxl, now in vesicles (vesicles/ AMIS stage); NHERF1 become cytoplasmic, before all three molecules recolocalized at the early forming (pre-apical patch [PAP]), and then open, lumen (Figures 3A and S3A, yellow arrowhead). A pool of pERM also transiently localized to the BL PM during Podxl transcytosis (Figure S3A, PAP, white arrows). This suggests that Podxl-NHERF1-Ezrin colocalize at the cell cortex, whether this be the ECM-abutting periphery or at the nascent lumen. The complex disassembles during polarity reorientation.

We examined the function of Podxl in lumenogenesis. Podxl depletion strongly perturbed SLF (Figure S3B), resulting in poorly formed or multiple lumens (Figure 3B), which was rescued by RNAi-resistant GFP-Podxl coexpression (Figures 3C–3E). In contrast to the robust AP localization of NHERF1, Ezrin, and pERM in control cysts (Figure 3B, arrows), Podxl depletion redistributed a pool of NHERF1 to the cytoplasm and Ezrin/pERM to the BL PM (Figure 3B, arrowheads), similar to their relocalization observed during Podxl transcytosis (Figure 3A). Podxl depletion also disrupted the normally luminal localization of additional AP proteins, Crumbs3a, Syntaxin-3a, and CNT1, which instead localized to Rab11a-positive vesicles beneath a presumptive AMIS (Figures S3A, S3C, and S3D, yellow arrowheads). Thus, Podxl is crucial for lumen formation and the AP localization of several proteins, including NHERF1 and Ezrin.

We observed that interaction with NHERF and ERM proteins was required for Podxl localization and AP-BL polarization. Expression of Podxl deficient in binding to either NHERF (PBM*) (Figure S3E) or ERM (FERM-binding motif mutant [FBM*]) proteins (Li et al., 2002; Schmieder et al., 2004) resulted in significantly decreased SLF, which was enhanced by codepletion of endogenous Podxl (Figures 3C–3E). AP targeting of both Podxl and Ezrin required the Podxl PBM. Upon Podxl PBM* expression, Ezrin and PBM-deficient Podxl localized to all cortical domains (white arrowheads) and PBM-deficient Podxl additionally to intracellular vesicles, some of which were quite large (Figure 3E, yellow arrowheads). In contrast, direct Ezrin interaction (uncoupled by FBM* mutant) was required for the SLF-promoting function of Podxl, but not the AP targeting of either Ezrin or Podxl (Figures 3D, arrows, and 3E). Expression of Podxl lacking both the FBM and PBM (Podxl FBM*/PBM*) was nonfunctional: it localized to subapical vesicles (yellow arrowheads), failed to rescue the BL mistargeting of Ezrin upon endogenous Podxl depletion (white arrowheads), and had no effect on SLF rates in either scramble or Podxl shRNA-expressing cysts (Figures 3C–3E). Thus, the entire Podxl-NHERF-ERM complex is required for mutual AP recruitment and cyst AP-BL polarity.

Podxl interacts with NHERF1/2 (Li et al., 2002; Schmieder et al., 2004). We previously identified both as required for SLF (Gálvez-Santisteban et al., 2012). ShRNAs to either NHERF significantly reduced SLF, with the greatest effect upon depletion of both, leading to vesicular Podxl accumulation (Figures 4A, yellow arrowheads, 4B, S3F, and S3G). This suggests nonredundant roles for NHERF1/2, which was supported by their differing localizations. NHERF1 colocalized with Podxl only at the PM, whether at the ECM-abutting surface or the AMIS/lumen (Figures 4C and S3H, white arrowheads). In contrast, NHERF2 only colocalized with Podxl during transcytosis in Rab11a-positive vesicles (Figures 4C and S3H, yellow arrowheads). Depletion of NHERF1 redistributed Podxl to NHERF2-positive vesicles (Figure 4C). Conversely, NHERF2 depletion redistributed a pool of NHERF1 to Podxl-positive vesicles. Domain mapping of NHERF1 confirmed that Podxl interacts with NHERF1 PDZ domain 2 (PDZ2) (Takeda et al., 2001) (Figure 4D). While both NHERF1 PDZ domains and NHERF-ERM interaction were required for SLF, the Podxl-interacting PDZ2 and FERM domain were required for efficient NHERF1 AP targeting (Figures 4E–4G). Thus, NHERF-1 and NHERF-2 function with Podxl in distinct locations. A ternary Podxl/NHERF1/ERM complex functions at the AP PM, while a Podxl-NHERF2 complex likely functions in endosomes.

In our system, Ezrin was a regulator of the cortical Podxl-NHERF1 complex, confirming previous studies (Fukasawa et al., 2011; Schmieder et al., 2004). Depletion of Ezrin significantly reduced SLF (Figure S3I) and caused vesicular accumulation of Podxl (Figure 4H, arrowheads). Ezrin depletion was rescued by RNAi-resistant WT GFP-Ezrin, which localized to the lumen (arrows), but not an inactive Ezrin mutant (phosphoinositide binding-deficient, PIP*; Figure 4I) (Fievet et al., 2004). Together, this suggests a PM complex of Podxl/NHERF1/Ezrin that is required for, and transiently dissociates during reorientation of, AP-BL polarity.

PKCβII Controls AP Polarization Independently of β1-Integrins

We examined how the Podxl-NHERF1-Ezrin complex is regulated during reorientation of cyst polarity. Classical protein kinase C (PKC) phosphorylation of the FBM in either Podxl (S481) or NHERF1 (S339,340) abolishes interaction of either protein with Ezrin (Chen et al., 2012; Fukasawa et al., 2011; Garbett et al., 2010). Classical PKC(s) may therefore regulate the transient disassembly of the Podxl complex during polarity reorientation (Figures 3A and S3A). We examined whether classical PKC inhibition, similar to Ezrin hyperphosphorylation (Figures 2K and 2M), accumulates a pool of Podxl at the ECM-abutting surface, thereby inducing front-rear polarization.

Treatment with pan-PKC inhibitor Gö-6983 caused accumulation of Podxl in vesicles close to the cell surface in the center of cysts (Figure S4A, arrowheads) and dose-dependent SLF decrease (Figure S4B). In contrast, classical PKC inhibitor Gö-6976, or PKCá pseudosubstrate treatment not only perturbed SLF (Figure S4B), but strikingly increased front-rear polarity (Figures 5A, S4C, and S4D), as indicated by asymmetric localization of NHERF1 (arrowhead) and active β1-integrin (arrow). Multiday imaging of GFP-Podxl/RFP-Histone 2B (H2B)-expressing cysts revealed that the Podxl-labeled peripheral membranes are a bona fide collective “front.” In controls, ~24 hr after plating, GFP-Podxl had internalized and was located in the inner region of cysts, eventually becoming the lumen (Figure 5B, control, yellow arrowheads), with cysts developing near the site of their initial observation (Figure 5B, cyst trace). Classical PKC-inhibited cysts, however, mirrored β1-integrin inhibition, developing collective motility (Figure 5B, cyst trace) and displaying a Podxl-decorated collective front, from which the directionality of migration always occurred (Figure 5B, +Gö-6976, white arrowheads). These data confirm that inhibition of PKC results in an inability to reorient polarity from initially inverted to luminally polarized, thereby inducing the development of collective front-rear motility.

To determine the specific classical PKC(s) involved, we depleted two major Gö-6976 targets: PKCα/β. Depletion of PKCβ severely reduced SLF and robustly increased front-rear polarity (Figures 5C–5G), mirroring Gö-6976 treatment (Figures S4B–S4D). PKCβ has two spliceforms: PKCβI and PKCβII (Rosse et al., 2010). PKCβ depletion was rescued by RNAi-resistant PKCβII (Figures 5E–5G), whereas ectopic PKCβI expression perturbed SLF and induced front-rear polarization irrespective of kinase activity or endogenous PKCβ depletion (Figures S5A– S5C). In contrast, PKCα depletion, either alone or in combination with RNAi-resistant kinase-dead PKCα (GFP-PKCα D463N) (Cameron et al., 2009), while significantly reducing SLF, only modestly increased front-rear polarization (Figures 5D, 5E, S4E, and S4G–S4K). PKCα/β codepletion did not significantly enhance the defects observed upon PKCβ depletion alone (Figures 5D and 5E). Therefore, PKCβII is likely the major polarity orientation-regulating classical PKC in MDCK cysts. Accordingly PKCβII overexpression reduced the baseline level of front-rear polarization (Figure 5G, hash symbol).

GFP-PKCβII localized to all cortical domains (Figure 5E, AP, yellow arrowheads; BL, arrows) and to intracellular vesicles (white arrowheads). However, active PKCβII, phosphorylated either on activation loop (T500, T641) or autophosphorylation (S660) sites, was detected primarily at the BL PM (arrows), in some vesicles (white arrowheads), with

minor levels at the AP PM marked by Podxl (Figures 5H and S5E, yellow arrowheads; see Experimental Procedures). Active PKCβII is thus localized to the appropriate PM to perturb the ECM-abutting localization of the Podxl complex. Although we expected that β1-integrin would control PKCα/β coactivation, we found that the activation and membrane recruitment of either PKCα or PKCβII was independent of β1-integrin. Inhibition, depletion, or mutational activation of β1-integrin, although affecting polarity orientation (Figure 1), failed to perturb PKCα or PKCβII activation or recruitment to the ECM-abutting surface (Figures 5H–5J, S4L, and S4M). These data indicate, surprisingly, that PKCβII is active under all conditions examined, irrespective of β1-integrin activation. Rather, the function of PKCα/βII in polarity orientation appears sequential to, and dependent on, prior downregulation of the RhoA pathway.

We thus probed the interplay between the classical PKC and RhoA pathways. Inhibition of RhoA and classical PKCs had opposing effects on polarity (Figures 6A–6C). PKC inhibition perturbed SLF and induced front-rear polarization. RhoA depletion abolished the already low baseline of front-rear polarization in control cysts (indicated by the hash sign; Figure 6C). Simultaneous RhoA/PKC perturbation returned SLF to control levels and significantly attenuated front-rear polarization. These data suggest that RhoA and PKCβII function in opposing pathways controlling polarization, potentially converging on the regulation of Ezrin association with the Podxl complex; RhoA-ROCKI may promote, while PKC potentially opposes, Ezrin association with Podxl-NHERF1.

To directly test this possibility, we first determined that PKCβ was a major regulator of Podxl complex phosphorylation using phosphorylation-specific antibodies to the NHERF1 FBM (pS339,340) (Chen et al., 2012). PKCβ, and to a lesser extent PKCα, depletion reduced PMA-induced phosphorylation of the FBM of endogenous NHERF1 (Figure 6F). Next, we expressed Podxl and NHERF1 PKC phosphorylation site mutants that control Ezrin association (Chen et al., 2012; Fukasawa et al., 2011). Expression of phosphorylation-deficient Podxl or NHERF1 strongly reduced SLF and induced front-rear polarization, which was potentiated by codepletion of endogenous Podxl/NHERF1. This occurred in a dose-dependent fashion for all NHERF1 PKC sites tested (Figures 6G–6L). Phosphorylation- deficient mutants of Podxl and NHERF1, which showed strong overlap with each other and Ezrin, localized predominantly to the collective front (arrows), or to poorly formed lumens (Figures 6G, 6J, S6A, and S6B). These data support the function of RhoA and PKCβII as opposing pathways promoting or inhibiting, respectively, front-rear polarization, through modulation of Ezrin association with Podxl/NHERF1.

The Podxl-NHERF1-Ezrin complex, although requiring disassembly at the ECM-abutting PM, requires subsequent reassembly at the AMIS for AP-BL polarization (Figures 3 and 4). Accordingly, expression of phosphomimetic mutants of Podxl or NHERF1 strongly perturbed SLF, without affecting front-rear polarization (Figures 6G–6L). Mimicking the transient dissociation of the complex during normal polarity reorientation (Figures 3A and S3A), phosphomimetic Podxl localized largely to intracellular vesicles that did not label for Ezrin (white arrowheads) or to poorly formed lumens (Figure 6G), while phosphomimetic NHERF1 became cytoplasmic upon triple Ser-to-Asp mutation (3×SD; Figure 6J). These

data reveal that Podxl complex phosphorylation represses its cortical localization and that phosphorylation must be reversed to allow complex reformation at the AMIS.

The PP2A phosphatase complex binds and dephosphorylates NHERF1 (Boratkó et al., 2012; Chen et al., 2012). We examined the localization of the NHERF1-associating PP2A-B55α subunit (3×HA-PP2A-Bα). At the initially inverted two-cell stage when Podxl was peripheral, we detected no specific colocalization with PP2A-Bα (Figures 7A and 7B). However, when vesicles containing Podxl began to accumulate at the AMIS (here marked by the polarity protein Par3, yellow arrowhead) (Bryant et al., 2010), corecruitment of PP2A-Bα could be observed (white arrowheads). As the lumen formed and Par3 redistributed to juxtaluminal puncta, PP2A-Bα continued to overlap with Podxl at the luminal PM (Figure 7B, arrows). Notably, depletion of PP2A-Bα mimicked the expression of phosphomimetic NHERF1 and Podxl, reducing SLF, causing the accumulation of Podxl in intracellular vesicles (arrowheads) and the cytoplasmic redistribution of NHERF1 (Figures 7C–7F; data not shown). These data reveal that PP2A functions in the establishment of AP-BL polarity by regulating the reformation of the Podxl-NHERF1-Ezrin complex at the AMIS.

DISCUSSION

Here, we elucidate a molecular switch that determines the orientation of polarity in the simple system of 3D MDCK cyst polarization. Initially, at the one- to two-cell stage, Podxl is at the ECM-abutting surface and polarity is inverted. During normal cyst formation, polarity is reoriented as Podxl internalizes and transcytoses to the AMIS, which eventually becomes the lumen. If components of the polarity reorientation switch mechanism are blocked, polarity inversion is largely maintained and multicellular aggregates with front-rear polarity form. During cyst formation a low, baseline percentage (6% ± 2%) of front-rear polarized aggregates occurs, indicating that transitions between these two types of polarity normally occur during polarization. In our previous work, when cysts were embedded in type-I collagen instead of grown on top of Matrigel, inhibition of β1-integrin gave almost complete inversion of polarity, with little or no front-rear polarity (Yu et al., 2005, 2008). The laminin in Matrigel partially rescues AP-BL polarity (O'Brien et al., 2001), supporting the notion that different ECM compositions regulate the type of polarity orientation and the collective behavior of epithelial cells (i.e., fully inverted or front-rear polarized).

The inverted localization of the Podxl-NHERF1-pEzrin complex is stabilized by elevated RhoA/ROCKI-dependent phosphorylation of Ezrin, which probably acts via a positive feedback loop to stabilize RhoA-ROCKI-pEzrin (Figure 7G, box 1) (Schmieder et al., 2004). Polarity is reoriented by locally inactivating RhoA at the ECM interface. α2/α3/β1-integrin complexes sense the ECM to activate FAK/p190ARhoGAP-dependent RhoA-GTP hydrolysis (Figure 7G, box 2) and decrease Ezrin phosphorylation. PKCβII phosphorylation of Podxl and NHERF1 dissociates them from Ezrin, triggering removal of Podxl from the periphery via endocytosis (Figure 7G, box 3). Internalized Podxl transcytoses to the AMIS (Bryant et al., 2010), likely now in association with NHERF2 (Figure 7G, box 4). The Podxl- NHERF1-Ezrin complex reforms at the AMIS via corecruitment of phosphatase PP2A (Figure 7G, box 5), probably promoting dephosphorylation of Podxl-NHERF1

(Boratkó et al., 2012; Chen et al., 2012). The AMIS then progresses to an open lumen, surrounded by a monolayer of AP-BL polarized epithelial cells. Thus, the ECM controls a molecular switch that determines reorientation from front-rear to AP-BL polarity by first inducing transient disassembly of the Podxl-NHERF1-pEzrin complex at the ECM-abutting PM.

At the earliest stage of cyst development (1–2 cells), the structures are highly motile, although motility ends concurrently with endocytosis of Podxl and the initiation of reorientation of polarity. When inverted polarity persists, structures remain motile, even though they can contain many cells. There are few cell culture model systems for studying collective cell motility, which consequently is much less well understood, compared to single cell motility. Our discovery of collective motility in this system offers opportunities for dissecting the molecular mechanisms underlying such behaviors.

In this system, collective motility is led by AP PM membrane components, rather than the expected integrin-decorated BL domain. This was dependent on the RhoA-ROCKI-Ezrin pathway, normally repressed by β1-integrins. β1-integrin-independent migration has been described in both cancer cells in 3D matrices and in dendritic cells in vivo, with such migration critically dependent on the RhoA-ROCK pathway (Lämmermann et al., 2008; Renkawitz et al., 2009; Tozluoğlu et al., 2013; Wyckoff et al., 2006). In 3D culture, the mode of migration can switch in a single cell type, dependent on the balance between RhoA/Rac1 mutual antagonism (Sanz-Moreno and Marshall, 2010). Our system also depends on the Rac1/RhoA balance, and our data suggest that cell surface asymmetry, including apical membrane-lead front-rear polarization, may contribute to such polarity switching in 3D. In our system, RhoA-GTP levels were highest at the ECM interface. RhoA-GTP at the front of invasive cysts may stabilize AP proteins, such as by activating ERM proteins and regulating their actin attachment. However, it is important to note that RhoA-ROCKI were dispensable for lumen formation, suggesting that there are additional mechanisms to stabilize Podxl-NHERF1-pERM at the lumen.

Ezrin association with the Podxl complex was critical for stabilization of the complex at the PM, whether at the ECM-abutting PM in inverted aggregates, or at the lumen. PKCβII triggered Podxl endocytosis and transcytosis to the AMIS. In all of our studies PKCβII activation was, unexpectedly, independent of β1-integrin activation, acting sequentially to RhoA-ROCKI pathway downregulation. This suggests a model (Figure 7G) whereby cortical stabilization of the Podxl-NHERF1-pEzrin complex by RhoA-ROCKI may allow the complex to become refractory to the always-active PKCβII; the actions of PKCβII only occur once integrin engagement leads to the lowering of pERM levels. The termination of PKC-mediated phosphorylation of Podxl-NHERF1 was critical for SLF and reassembly of Podxl- NHERF1-Ezrin at the AMIS. This appeared to be mediated by the phosphatase PP2A, in accordance with its role as a major NHERF1 phosphatase (Chen et al., 2012; Garbett et al., 2010). Thus, pathways that converge on Ezrin association or dissociation with the Podxl, or perhaps other AP, complex(es) may control collective epithelial polarization by modulating the cortical stabilization of ERM-interacting proteins.

It is important to note that the RhoA-inhibitory and PKC pathways described here do not promote formation of the BL PM per se, but rather repress formation of AP PM, giving positional coordinates that prevent peripheral Podxl stabilization. If destabilized at the PM, Podxl undergoes endocytosis and trancytosis to the AMIS. This involves a complex network of trafficking machinery masterminded by the Rab11a GTPase, and a myriad of additional GTPases and their effectors, to ensure the fidelity of transport of Podxl-containing vesicles precisely to the AP PM (Bryant et al., 2010; Gálvez-Santisteban et al., 2012; Roland et al., 2011). That the AP PM can be either the lumen or the “front” of migrating aggregates suggests that the directionality of the apical membrane transport machinery must also be a target of ECM-derived signals. More generally, the switch mechanism uncovered here depends on the balance between the opposing forces of the multiple kinases and complexes that we elucidate. This likely forms the basis for the bistability between the inverted and luminal AP-BL polarity forms and potentially serves as a prototype for understanding how the orientation of polarity occurs in many other types of polarized systems. Whether this switch is bidirectional and AP PM components can be switched “back” to the ECM-abutting membrane after luminal polarity has formed is an important future question.

The molecular mechanisms were present here are likely to model many, but not all, signaling pathways controlling cell polarization. For instance, mammary epithelia, although normally a bilayer in vivo, transduce polarity orientation apparently through the pseudokinase ILK (Akhtar and Streuli, 2013), rather than the FAK- and Rac1-dependent pathways we describe, when cultured as a 3D monolayered acinus in vitro. This contrasts with the monolayer found both in MDCK and kidney epithelia in vivo. Moreover, in colon cancer cell 3D models and the developing mouse aorta Moesin, rather than Ezrin, is the major ERM protein required for lumen formation (Georgescu et al., 2014; Strilić et al., 2009). These may represent cell- or tissue-type differences in polarization mechanisms. Importantly, our data and the model we present does not preclude roles for Moesin and ILK in either front-rear or luminal polarization. As polarity reorientation and lumen formation occurs over days, there are likely many additional molecules and intermediate steps involved in the reorientation mechanism we describe.

EXPERIMENTAL PROCEDURES

Cyst Matrigel Culture

3D Matrigel culture of MDCK cysts was as previously described (Bryant et al., 2010). Briefly, cells subcultured in 5% fetal bovine serum (FBS; GIBCO), minimum essential medium (MEM) were trypsinized to a single cell suspension at 1.5×10^4 cells ml^{-1} in complete medium containing 2% Matrigel (BD Biosciences). Cell-medium-Matrigel suspensions (300 μl) were plated into 8-well coverglass chambers (Nunc, LabTek-II), precoated with 5 μl of 100% Matrigel. Cells were grown for 24–48 hr before fixation in4%paraformaldehyde (PFA). In some experiments, cells were treated with Gö-6976, Gö-6983 (Calbiochem), or equal volume of DMSO as a control from the time of plating. In all instances, exogenous proteins were from stably expressing cell lines, created either by DNA lipofection, or retroviral infection, followed by selection for 1–3 weeks and FACS to obtain appropriate expression levels. All selective antibiotics were removed 24 hr prior to

plating for 3D culture. For AIIB2 treatments, the antibody was added to the culture medium in a final concentration of 8 μg/ml. For ROCK inhibition, Y-27632 (10 μM) was added at the time of plating and refreshed every 2 days.

Statistics

Single lumen formation quantification was adapted from as previously described (Bryant et al., 2010). Briefly, cysts were scored into three categories: (1) cyst with Podxl at a single lumen, (2) a cyst with peripherally located Podxl, or (3) multiple lumens/vesicular Podxl accumulation. For RNAi rescue experiments, only cysts expressing detectable levels of the exogenous transgene by confocal microscopy were scored. The relative percentages of cysts from each category were normalized to control cysts. Values are mean ± SD from three replicate experiments, with $n \geq 100$ cysts per replicate. Significance was calculated using a paired, two-tailed Student's t test. Line-scan analysis for pixel intensity was performed using Zeiss LSM510 imaging software and graphed using Microsoft Excel.

Time-Lapse Phase Movies

Cells grown in Matrigel-coated 24-well plates were imaged essentially as previously described (Yu et al., 2007), using a Zeiss Axiovert S-100 microscope (Carl Zeiss). AIIB2 was added at the time of plating, where appropriate. Time-lapse movies were recorded from 3–169 hr after plating. Imaging specifications include: a 10× A-Plan objective lens, a Cohu high-performance charge-coupled device camera, light exposure regulated though a Ludl shutter, controller and x-y-z–motorized stage. A 37°C temperature and 5% carbon dioxide environment were maintained via a CTI Controller 3700 and Temperature Control 37.2 combination (Carl Zeiss). Images were acquired at 15 min intervals using a custom macro implemented in OpenLab 4.0.2 (Improvision). Images were recorded using OpenLab LIFF series (Improvision) and compiled into QuickTime movies via ImageJ (NIH). Cyst outlines were traced in Adobe Illustrator from still frames every 12 hr from 16–132 hr after plating.

Live Cell Dual-Color Imaging

Cells were plated as described above, although adjusted to 2-well chamber slides (Labtek II, Nunc). Cells coexpressing EGFP-Podxl/RFP-H2B were imaged on an inverted spinning-disk confocal microscope system (Yokogawa/ Zeiss) with a 37°C and 5% CO_2 controlled environment (Zeiss) and heated stage (PECON) through a 20× 1.49NA lens (Zeiss), using 488/561 nm laser lines. Images were captured via an AxioCam Mrm (Zeiss). A stack of three images at 5 μm intervals were taken every 30 min from 16–76.5 hr after plating using an automated stage controlled via the ZEN software package (Zeiss). As cysts develop and move during image acquisition, the optimal focal plane was manually chosen for each time point postacquisition from the stacked images, before compilation of image series of each movie. Movies were processed using ImageJ (NIH). For PKC inhibition, Gö-6976 (0.5 μM) was added at the time of plating. Cyst outlines were traced in Adobe Illustrator from still frames every 2 hr from 24–52 hr after plating.

Materials and procedures for RNAi, virus production and transduction, plasmids and cell lines, and antibodies and immunolabeling are detailed in the Supplemental Experimental Procedures.

Supplementary Material

Refer to Web version on PubMed Central for supplementary material.

Acknowledgments

We thank the investigators who kindly gifted reagents and the K.E.M. laboratory for assistance. This work was supported by an American Cancer Society Research Scholar Grant (RSG-12-141-01-CSM to A.J.E.), and NIH grants K99CA163535 (D.B.), R01CA057621 (Z.W.), R01DK074398 (K.M.), and R01DK091530 (K.M.).

REFERENCES

Akhtar N, Streuli CH. An integrin-ILK-microtubule network orients cell polarity and lumen formation in glandular epithelium. Nat. Cell Biol. 2013; 15:17–27. [PubMed: 23263281]

Apodaca G, Gallo LI, Bryant DM. Role of membrane traffic in the generation of epithelial cell asymmetry. Nat. Cell Biol. 2012; 14:1235–1243. [PubMed: 23196841]

Bigorgne AE, Farin HF, Lemoine R, Mahlaoui N, Lambert N, Gil M, Schulz A, Philippet P, Schlesser P, Abrahamsen TG, et al. TTC7A mutations disrupt intestinal epithelial apicobasal polarity. J. Clin. Invest. 2014; 124:328–337. [PubMed: 24292712]

Boratkó A, Gergely P, Csortos C. Cell cycle dependent association of EBP50 with protein phosphatase 2A in endothelial cells. PLoS ONE. 2012; 7:e35595. [PubMed: 22523604]

Bryant DM, Mostov KE. From cells to organs: building polarized tissue. Nat. Rev. Mol. Cell Biol. 2008; 9:887–901. [PubMed: 18946477]

Bryant DM, Datta A, Rodríguez-Fraticelli AE, Peränen J, Martín-Belmonte F, Mostov KE. A molecular network for de novo generation of the apical surface and lumen. Nat. Cell Biol. 2010; 12:1035–1045. [PubMed: 20890297]

Cameron AJ, Escribano C, Saurin AT, Kostelecky B, Parker PJ. PKC maturation is promoted by nucleotide pocket occupation independently of intrinsic kinase activity. Nat. Struct. Mol. Biol. 2009; 16:624–630. [PubMed: 19465915]

Chen JY, Lin YY, Jou TS. Phosphorylation of EBP50 negatively regulates β-PIX-dependent Rac1 activity in anoikis. Cell Death Differ. 2012; 19:1027–1037. [PubMed: 22301917]

Datta A, Bryant DM, Mostov KE. Molecular regulation of lumen morphogenesis. Curr. Biol. 2011; 21:R126–R136. [PubMed: 21300279]

deLeon O, Puglise JM, Liu F, Smits J, ter Beest MB, Zegers MM. Pak1 regulates the orientation of apical polarization and lumen formation by distinct pathways. PLoS ONE. 2012; 7:e41039. [PubMed: 22815903]

Doyonnas R, Kershaw DB, Duhme C, Merkens H, Chelliah S, Graf T, McNagny KM. Anuria, omphalocele, and perinatal lethality in mice lacking the CD34-related protein podocalyxin. J. Exp. Med. 2001; 194:13–27. [PubMed: 11435469]

Fehon RG, McClatchey AI, Bretscher A. Organizing the cell cortex: the role of ERM proteins. Nat. Rev. Mol. Cell Biol. 2010; 11:276–287. [PubMed: 20308985]

Ferrari A, Veligodskiy A, Berge U, Lucas MS, Kroschewski R. ROCK-mediated contractility, tight junctions and channels contribute to the conversion of a preapical patch into apical surface during isochoric lumen initiation. J. Cell Sci. 2008; 121:3649–3663. [PubMed: 18946028]

Fievet BT, Gautreau A, Roy C, Del Maestro L, Mangeat P, Louvard D, Arpin M. Phosphoinositide binding and phosphorylation act sequentially in the activation mechanism of ezrin. J. Cell Biol. 2004; 164:653–659. [PubMed: 14993232]

Fukasawa H, Obayashi H, Schmieder S, Lee J, Ghosh P, Farquhar MG. Phosphorylation of podocalyxin (Ser415) Prevents RhoA and ezrin activation and disrupts its interaction with the actin cytoskeleton. Am. J. Pathol. 2011; 179:2254–2265. [PubMed: 21945805]

Gálvez-Santisteban M, Rodriguez-Fraticelli AE, Bryant DM, Vergarajauregui S, Yasuda T, Bañón-Rodríguez I, Bernascone I, Datta A, Spivak N, Young K, et al. Synaptotagmin-like proteins control the formation of a single apical membrane domain in epithelial cells. Nat. Cell Biol. 2012; 14:838–849. [PubMed: 22820376]

Garbett D, LaLonde DP, Bretscher A. The scaffolding protein EBP50 regulates microvillar assembly in a phosphorylation-dependent manner. J. Cell Biol. 2010; 191:397–413. [PubMed: 20937695]

Georgescu MM, Cote G, Agarwal NK, White CL 3rd. NHERF1/EBP50 Controls Morphogenesis of 3D Colonic Glands by Stabilizing PTEN and Ezrin-Radixin-Moesin Proteins at the Apical Membrane. Neoplasia. 2014; 16:365–374. e362. [PubMed: 24862762]

Ichimura K, Powell R, Nakamura T, Kurihara H, Sakai T, Obara T. Podocalyxin regulates pronephric glomerular development in zebrafish. Physiological reports. 2013; 1

Jou TS, Nelson WJ. Effects of regulated expression of mutant RhoA and Rac1 small GTPases on the development of epithelial (MDCK) cell polarity. J. Cell Biol. 1998; 142:85–100. [PubMed: 9660865]

Lämmermann T, Bader BL, Monkley SJ, Worbs T, Wedlich-Söldner R, Hirsch K, Keller M, Förster R, Critchley DR, Fässler R, Sixt M. Rapid leukocyte migration by integrin-independent flowing and squeezing. Nature. 2008; 453:51–55. [PubMed: 18451854]

Li Y, Li J, Straight SW, Kershaw DB. PDZ domain-mediated interaction of rabbit podocalyxin and Na(+)/H(+) exchange regulatory factor-2. Am. J. Physiol. Renal Physiol. 2002; 282:F1129–F1139. [PubMed: 11997330]

Murakoshi H, Wang H, Yasuda R. Local, persistent activation of Rho GTPases during plasticity of single dendritic spines. Nature. 2011; 472:100–104. [PubMed: 21423166]

O'Brien LE, Jou TS, Pollack AL, Zhang Q, Hansen SH, Yurchenco P, Mostov KE. Rac1 orientates epithelial apical polarity through effects on basolateral laminin assembly. Nat. Cell Biol. 2001; 3:831–838. [PubMed: 11533663]

Paszek MJ, Zahir N, Johnson KR, Lakins JN, Rozenberg GI, Gefen A, Reinhart-King CA, Margulies SS, Dembo M, Boettiger D, et al. Tensional homeostasis and the malignant phenotype. Cancer Cell. 2005; 8:241–254. [PubMed: 16169468]

Renkawitz J, Schumann K, Weber M, Lämmermann T, Pflicke H, Piel M, Polleux J, Spatz JP, Sixt M. Adaptive force transmission in amoeboid cell migration. Nat. Cell Biol. 2009; 11:1438–1443. [PubMed: 19915557]

Roland JT, Bryant DM, Datta A, Itzen A, Mostov KE, Goldenring JR. Rab GTPase-Myo5B complexes control membrane recycling and epithelial polarization. Proc. Natl. Acad. Sci. USA. 2011; 108:2789–2794. [PubMed: 21282656]

Rosse C, Linch M, Kermorgant S, Cameron AJ, Boeckeler K, Parker PJ. PKC and the control of localized signal dynamics. Nat. Rev. Mol. Cell Biol. 2010; 11:103–112. [PubMed: 20094051]

Sanz-Moreno V, Marshall CJ. The plasticity of cytoskeletal dynamics underlying neoplastic cell migration. Curr. Opin. Cell Biol. 2010; 22:690–696. [PubMed: 20829016]

Schmieder S, Nagai M, Orlando RA, Takeda T, Farquhar MG. Podocalyxin activates RhoA and induces actin reorganization through NHERF1 and Ezrin in MDCK cells. J. Am. Soc. Nephrol. 2004; 15:2289–2298. [PubMed: 15339978]

Strilić B, Kucera T, Eglinger J, Hughes MR, McNagny KM, Tsukita S, Dejana E, Ferrara N, Lammert E. The molecular basis of vascular lumen formation in the developing mouse aorta. Dev. Cell. 2009; 17:505–515. [PubMed: 19853564]

Strilić B, Eglinger J, Krieg M, Zeeb M, Axnick J, Babál P, Müller DJ, Lammert E. Electrostatic cell-surface repulsion initiates lumen formation in developing blood vessels. Curr. Biol. 2010; 20:2003–2009. [PubMed: 20970336]

Takeda T, Go WY, Orlando RA, Farquhar MG. Expression of podocalyxin inhibits cell-cell adhesion and modifies junctional properties in Madin-Darby canine kidney cells. Mol. Biol. Cell. 2000; 11:3219–3232. [PubMed: 10982412]

Takeda T, McQuistan T, Orlando RA, Farquhar MG. Loss of glomerular foot processes is associated with uncoupling of podocalyxin from the actin cytoskeleton. J. Clin. Invest. 2001; 108:289–301. [PubMed: 11457882]

Tomar A, Lim ST, Lim Y, Schlaepfer DD. A FAK-p120RasGAP-p190RhoGAP complex regulates polarity in migrating cells. J. Cell Sci. 2009; 122:1852–1862. [PubMed: 19435801]

Tozluoğlu M, Tournier AL, Jenkins RP, Hooper S, Bates PA, Sahai E. Matrix geometry determines optimal cancer cell migration strategy and modulates response to interventions. Nat. Cell Biol. 2013; 15:751–762. [PubMed: 23792690]

Wyckoff JB, Pinner SE, Gschmeissner S, Condeelis JS, Sahai E. ROCK- and myosin-dependent matrix deformation enables protease- independent tumor-cell invasion in vivo. Curr. Biol. 2006; 16:1515–1523. [PubMed: 16890527]

Yu W, Datta A, Leroy P, O'Brien LE, Mak G, Jou TS, Matlin KS, Mostov KE, Zegers MM. Beta1-integrin orients epithelial polarity via Rac1 and laminin. Mol. Biol. Cell. 2005; 16:433–445. [PubMed: 15574881]

Yu W, Fang X, Ewald A, Wong K, Hunt CA, Werb Z, Matthay MA, Mostov K. Formation of cysts by alveolar type II cells in three-dimensional culture reveals a novel mechanism for epithelial morphogenesis. Mol. Biol. Cell. 2007; 18:1693–1700. [PubMed: 17332496]

Yu W, Shewan AM, Brakeman P, Eastburn DJ, Datta A, Bryant DM, Fan QW, Weiss WA, Zegers MM, Mostov KE. Involvement of RhoA, ROCK I and myosin II in inverted orientation of epithelial polarity. EMBO Rep. 2008; 9:923–929. [PubMed: 18660750]

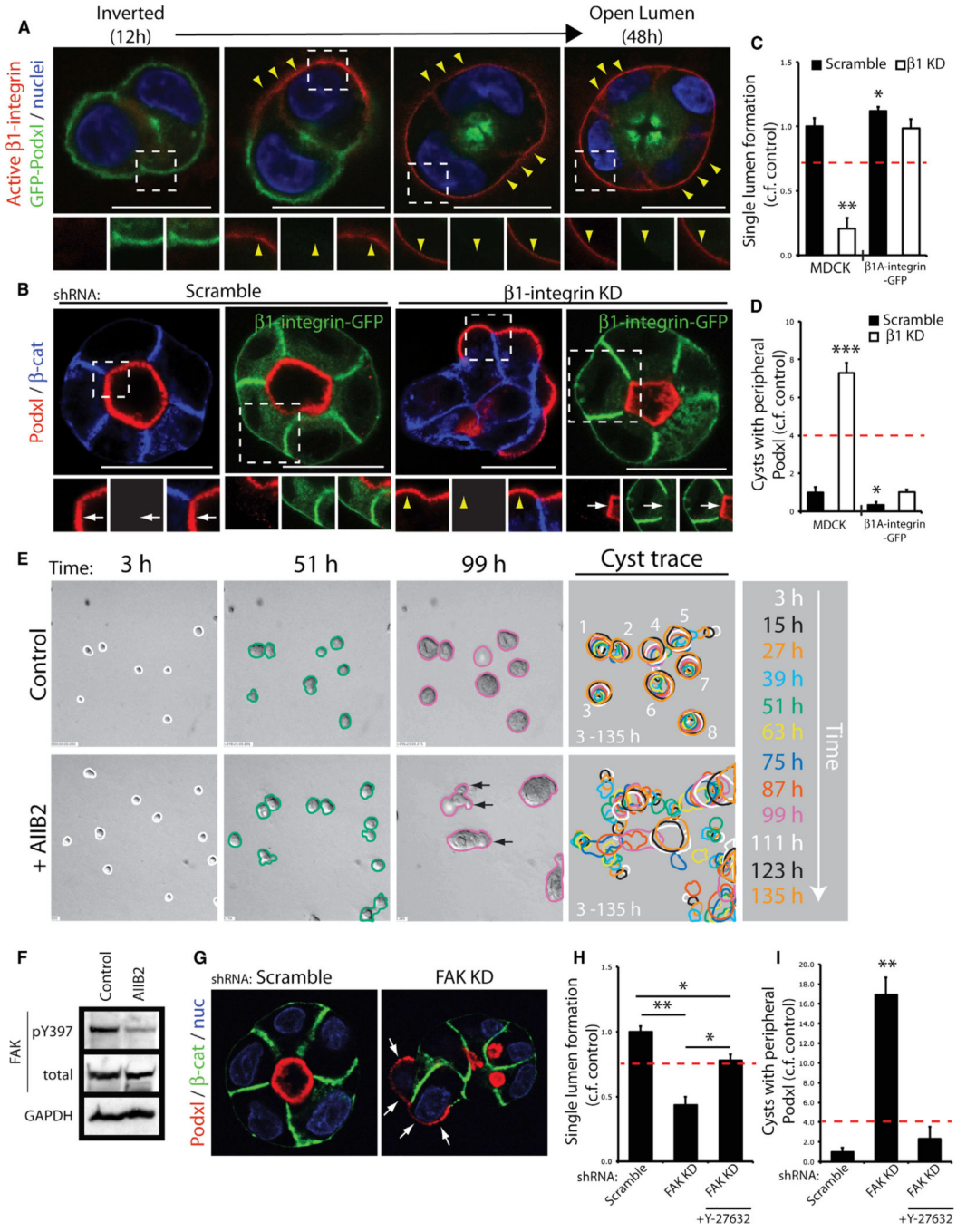

Figure 1. β1-Integrins Promote Luminal Polarity and Constrain Long-Range Motility in Cysts

(A) GFP-Podxl, active β1-integrin and nuclei localization during progression from initially inverted (12 hr) to open lumen cysts (48 hr). Arrowheads, basal. In all instances, bottom panels are higher magnification of split color images from boxed regions. Scale bars represent 20 μm (unless otherwise indicated).

(B) Parental or β1-integrin-GFP-expressing cysts with control or β1-integrin knockdown (KD) stained for Podxl and β-catenin. Arrows, AP; yellow arrowheads, peripheral. All cysts, 48 hr after plating, unless otherwise indicated.

(C and D) Quantitation SLF (C) or peripheral Podxl (D) (see Experimental Procedures) upon β1-integrin manipulation in parental (MDCK) or β1-integrin-GFP cells (mean ± SD, n≥100 cysts/condition/experiment, three independent experiments). Black bars, scramble shRNA; white bars β1-integrin KD. In all instances, the red dotted line is the threshold considered for a positive hit (SLF, <75% of control; peripheral Podxl,≥4-fold change over control). *p < 0.05, **p < 0.001, ***p > 0.0001.

(E) Still frames of phase-contrast imaging of control or β1-integrin-inhibited (+AIIB2) cysts (time indicated from time-lapse (every 15 min from 3–169 hr after plating)). Cyst outlines were traced from every 12 hr from 3–135 hr, indicated by alternating color. Arrows, collective front.

(F) Active FAK (pY397), total FAK, or GAPDH levels from total cell lysates of cysts without (control) or with (AIIB2) β1-integrin inhibition.

(G) Control or FAK-depleted cysts stained for Podxl, β-catenin and nuclei. Arrows, peripheral.

(H and I) Quantitation of SLF (H) or peripheral Podxl (I) upon control or FAK depletion, with or without Y-27632 (10 μM) inhibition (mean ± SD, n ≥ 100 cysts/condition/experiment, three independent experiments). Black bars, scramble shRNA; white bars, β1-integrin KD. See also Figure S1 and Movie S1.

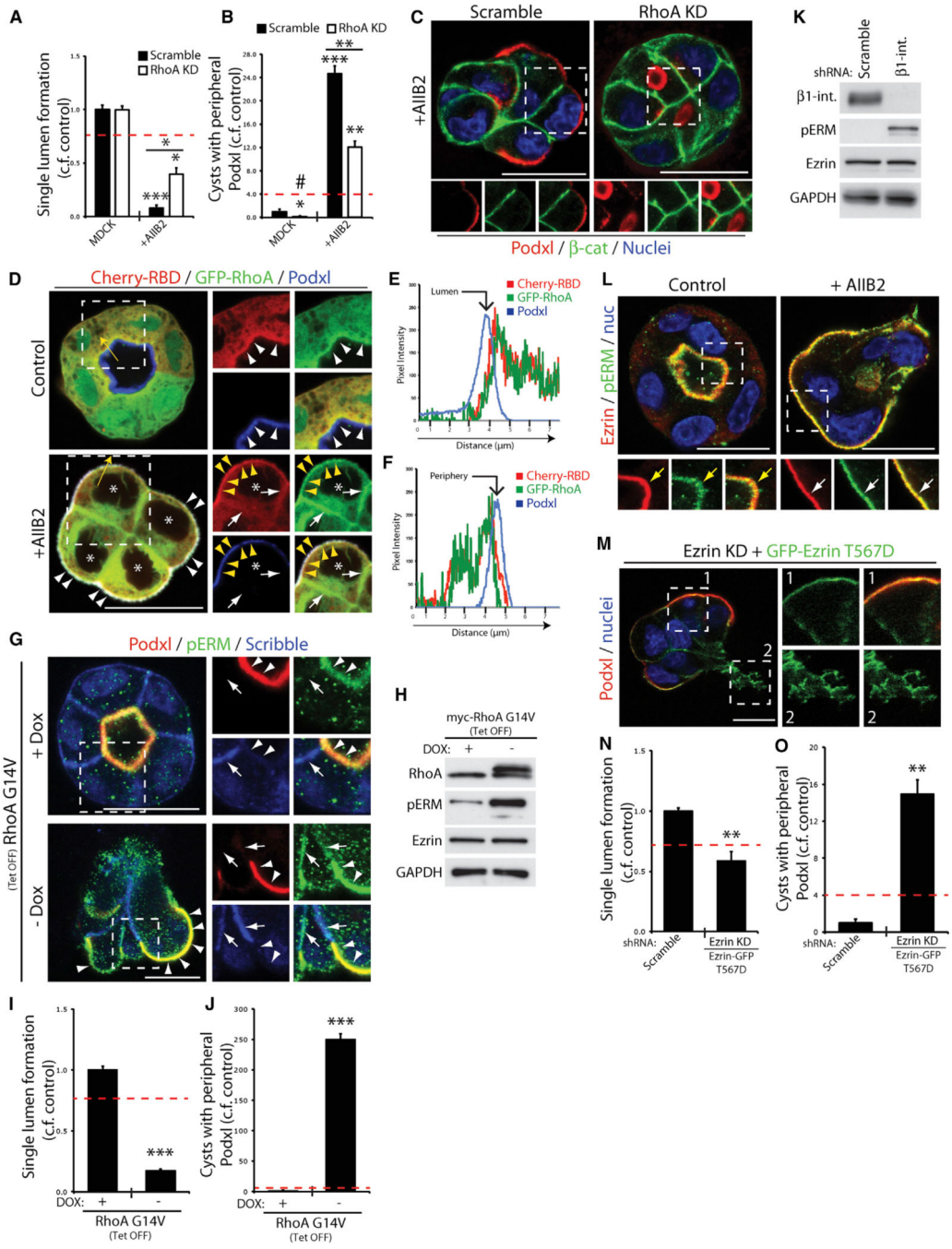

Figure 2. A RhoA-Ezrin Pathway Is Necessary and Sufficient for Front-Rear, but Not Luminal AP-BL, Polarity

(A and B) Quantitation of cyst SLF (A) or peripheral Podxl (B), upon control or β1-integrin inhibition (+AIIB2), with scramble (black bars) or RhoA (white bars) KD (mean ± SD, n ≥ 100 cysts/condition/experiment, three independent experiments). Hash symbol, value approaching zero.

(C) Cysts with scramble or RhoA KD stained for Podxl, β-catenin, and nuclei.

(D) Control or β1-integrin-inhibited (+AIIB2) cysts coexpressing GFP-RhoA and Cherry-tagged-RBD stained for Podxl. White arrowheads, AP; yellow arrowheads, peripheral;

arrows, lateral; asterisks, nuclei. Right panels: higher magnification of split-color images from boxed regions. Yellow arrows, line-scan region for (E) and (F).

(E and F) Quantitation of pixel intensity from line-scan regions in control (E) or AIIB2-treated (F) cysts.

(G) Cysts with repressed (+Dox) or induced (−Dox) RhoA G14V expression stained for Podxl, pERM, and Scribble. Arrowheads, AP; arrows, BL.

(H) RhoA (upper band, myc-tagged RhoA G14V), pERM, total Ezrin, and GAPDH levels from total cell lysates of cysts without (+DOX) or with (−Dox) myc-RhoA G14V expression.

(I and J) Quantitation of cysts with SLF (I) or peripheral Podxl (J) upon RhoA G14V repression (+Dox) or expression (−Dox) (mean ± SD, n≥100 cysts/condition/ experiment, three independent experiments).

(K) β1-integrin, pERM, total Ezrin, and GAPDH expression total cell lysates of cysts expressing scramble or β1-integrin KD.

(L) Cysts without (control) or with (+AIIB2) β1-integrin inhibition stained for Ezrin, pERM and nuclei. Yellow arrows, luminal; arrows, peripheral.

(M) Cysts coexpressing Ezrin shRNA and RNAi-resistant GFP-Ezrin T567D stained for Podxl and nuclei. Right panels: higher magnification of split red and green images from numbered, boxed regions.

(N and O) Quantitation of SLF (N) or peripheral Podxl (O) upon control (scramble shRNA) or Ezrin shRNA/RNAi-resistant GFP-Ezrin T567D coexpression (mean ± SD, n ≥ 100 cysts/condition/experiment, three independent experiments). See also Figure S2.

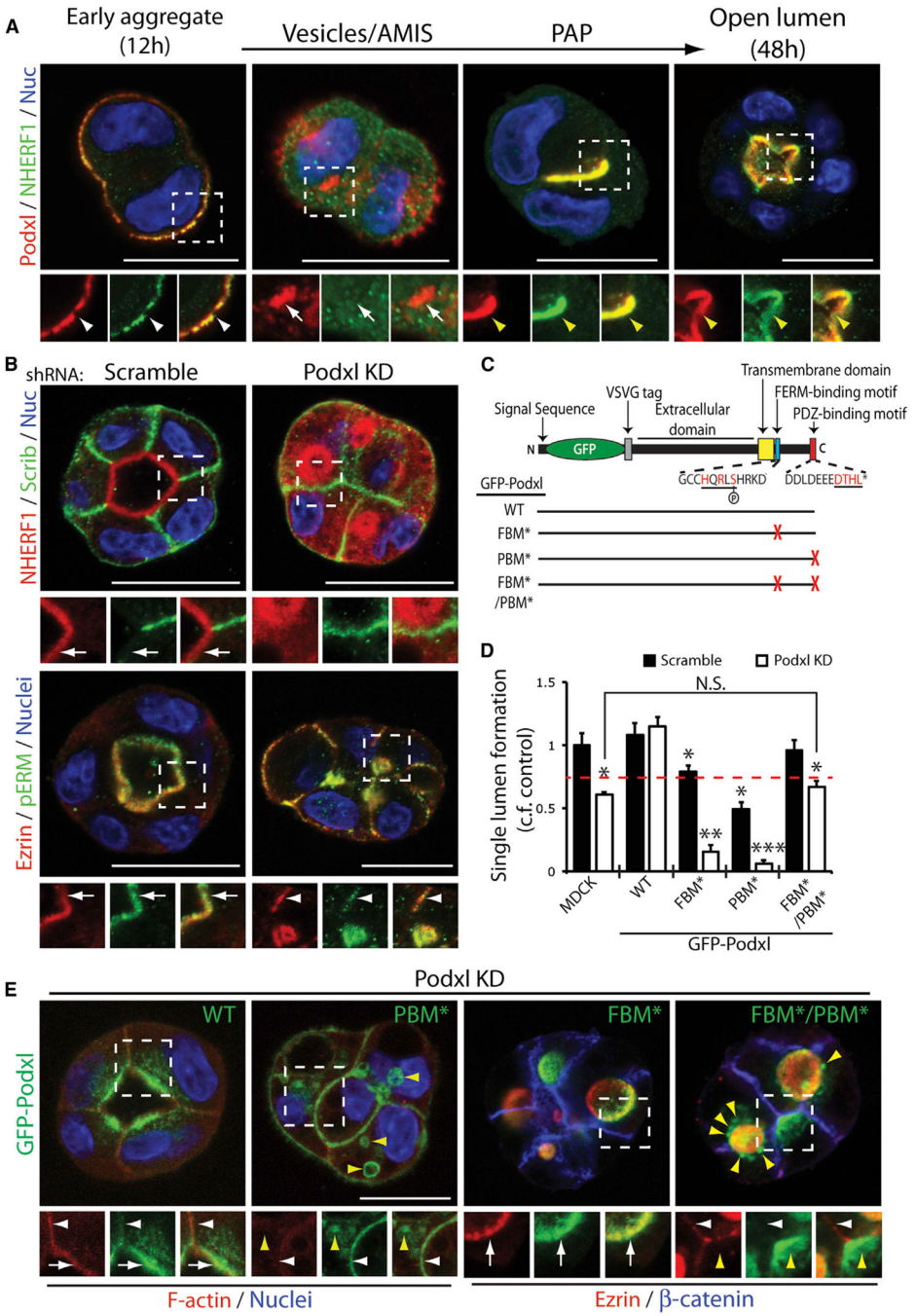

Figure 3. Podxl-NHERF-ERM Tail Interactions Are Required for AP-BL Polarization

(A) Podxl, NHERF1, and nuclei localization during lumen formation (12–48 hr). White arrowheads, peripheral; arrows, vesicular; yellow arrowheads, luminal. AMIS, AP membrane initiation site; PAP, pre-AP patch.

(B) Control (scramble KD) or Podxl KD cysts stained for nuclei and either (top) NHERF1 and Scribble, or (bottom) Ezrin and pERM. Arrows, luminal; arrowheads, lateral.

(C) Cartoon of GFP-Podxl domains and motifs. WT, wild-type; FBM*, FERM-binding motif mutant; PBM, PDZ-binding motif mutant.

(D) Quantitation of SLF in control (white bars) or Podxl KD (black bars) cysts without or with indicated RNAi-resistant GFP-Podxl domain mutant expression (mean ± SD, n ≥ 100 cysts/condition/experiment, three independent experiments).

(E) Cysts coexpressing Podxl KD and GFP-Podxl (green) wild-type (WT) or domain mutants stained for either (left two panels) F-actin and nuclei, or (right two panels) Ezrin and β-catenin. Arrows, luminal; yellow arrowheads, vesicular; white arrowheads, lateral.

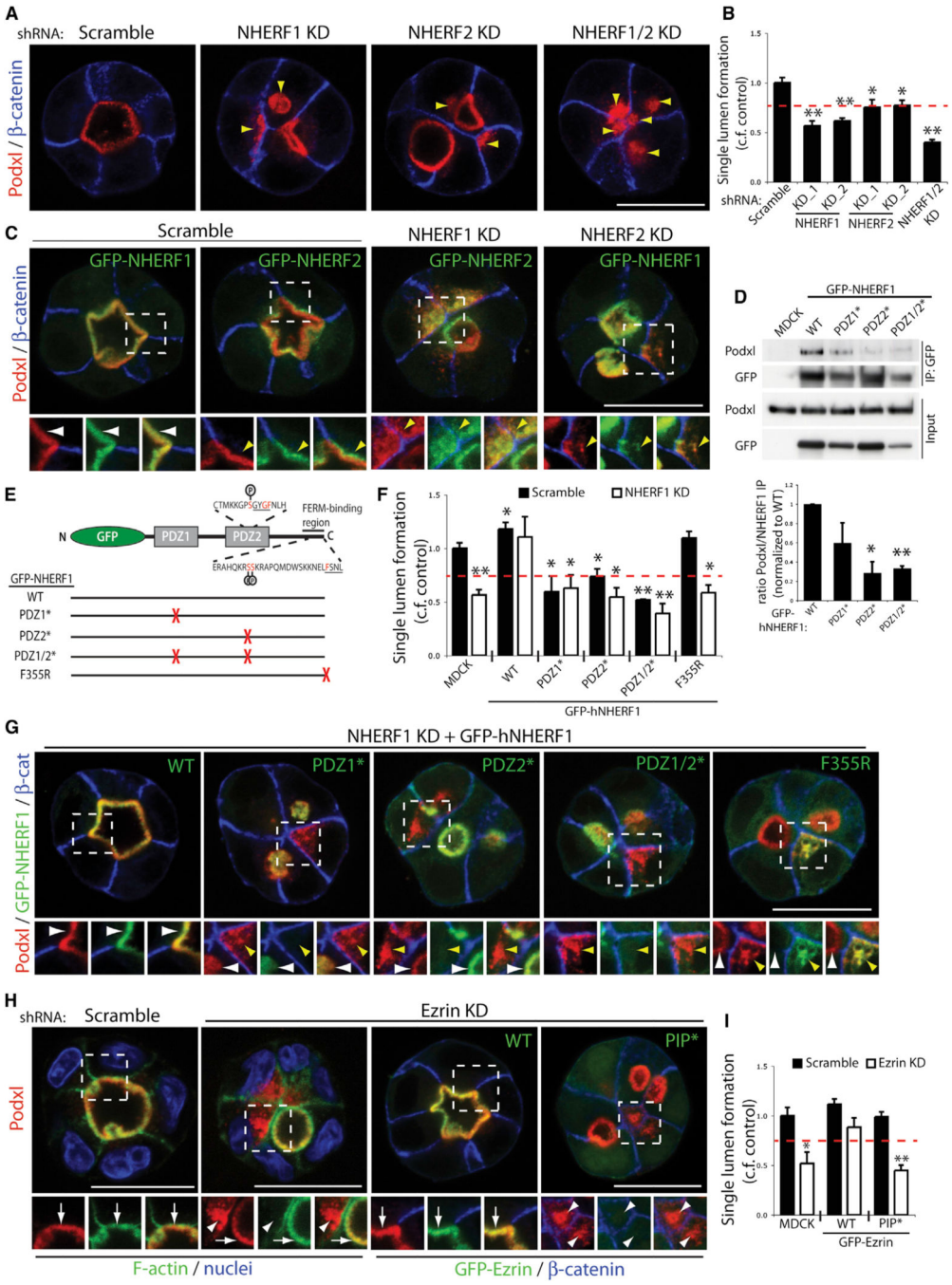

Figure 4. Formation of a Cortical Podxl-NHERF1-Ezrin Complex Regulates AP Domain Formation

(A) Cysts expressing either scramble (control), or single or dual NHERF1/2 shRNAs were stained for Podxl and β-catenin. Arrowheads, intracellular Podxl.

(B) Quantitation of cysts with SLF upon expression of scramble, NHERF1 or NHERF2 shRNAs, alone or in combination (mean ± SD, n ≥ 100 cysts/condition/ experiment, three independent experiments).

(C) Cysts coexpressing GFP-NHERF1 or GFP-NHERF2 (both green) and either Scramble, NHERF1, or NHERF2 shRNA stained for Podxl and β-catenin. White arrowheads, luminal; yellow arrowheads, vesicular.

(D) Lysates of control or GFP-NHERF1 wild-type and domain mutants immunoprecipitated with anti-GFP antibodies, were western blotted for total Podxl and GFP (input), and immunoprecipitated Podxl and GFP (IP: GFP). Band intensities are a ratio of immunoprecipitated Podxl/NHERF1, normalized to WT NHERF1. Values are mean ± SD from three experiments.

(E) Cartoon of GFP-NHERF1 domains and motifs. WT, wild-type; PDZ1*, PDZ domain 1 mutant; PDZ2*, PDZ domain 2 mutant; PDZ1/2*, PDZ domains 1 + 2 mutant; F355R, FERM-binding region mutant.

(F) Quantitation of SLF in control (black bars) or NHERF1 KD cysts (white bars), without or with indicated RNAi-resistant GFP-NHERF1 mutant expression (mean ± SD, n ≥ 100 cysts/condition/experiment, three independent experiments).

(G) Cysts coexpressing NHERF1 KD and RNAi-resistant GFP-NHERF1 wild-type (WT) or domain mutants (all green) stained for Podxl and β-catenin. White arrowheads, luminal; yellow arrowheads, vesicular.

(H) Cysts expressing either scramble or Ezrin KD and either RNAi-resistant GFP-Ezrin WT or a phosphoinositide binding-deficit (PIP*) mutant stained for Podxl and either (left two panels) F-actin and nuclei, or (right two panels) β-catenin. Arrows, luminal; arrowheads, vesicular.

(I) Quantitation of cysts with SLF upon control (black bars) or Ezrin (white bars), KD without or with RNAi-resistant GFP-Ezrin WT or PIP* expression (mean ± SD, n ≥ 100 cysts/condition/experiment, three independent experiments). See also Figure S3.

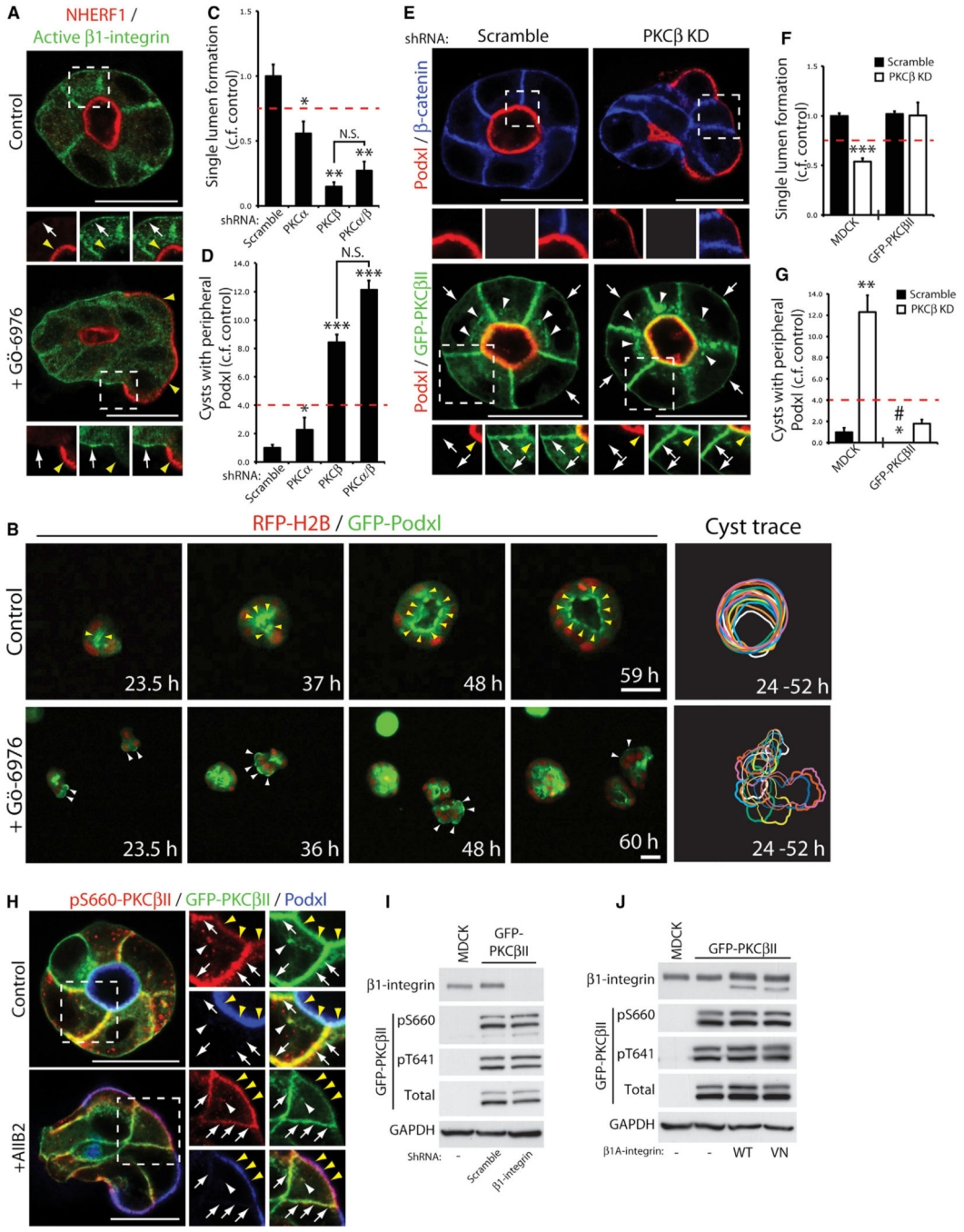

Figure 5. PKCβII Regulates Polarity Orientation

(A) Control or classical PKC-inhibited cysts (+Gö-6976, 0.5 μM) stained for Podxl and active β1-integrin. Arrowheads, Podxl; arrows, integrin.

(B) Time-lapse dual-color confocal imaging of cysts expressing RFP-H2B (nuclei) and GFP-Podxl without (control, top) or with PKC inhibition (+Gö-6976, 0.5 μM, bottom). Images were taken every 30 min from 16–76.5 hr after plating. Stills are presented from ~24–60 hr. Cyst outlines were traced from still frames every 2 hr (using alternating color), from 24–52 hr. Yellow arrowheads, luminal; White arrowheads, peripheral.

(C and D) Quantitation of SLF (C) or peripheral Podxl (D) in cysts upon control (scramble), or single or dual PKCα/β KD (mean ± SD, n ≥ 100 cysts/condition/ experiment, three independent experiments). N.S., not significant.

(E) Cysts expressing either scramble or PKCβ KD without (top panels) or with (bottom panels) coexpression of RNAi-resistant GFP-PKCβII (green) stained for Podxl (red) and β-catenin (blue). Insets show Podxl alone (left), GFP-PKCβII alone (middle), and merge (right). Arrows, BL; white arrowheads, vesicular; yellow arrows, AP.

(F and G) Quantitation of SLF (F) or peripheral Podxl (G) in cysts upon control (black bars) or PKCβ KD (white bars) without (MDCK) or with GFP-PKCβII coexpression (mean ± SD, n ≥ 100 cysts/condition/experiment, three independent experiments). Hash symbol, abolished front-rear polarity.

(H) Cysts expressing GFP-PKCβII without (top, control) or with (bottom, +AIIB2) β1-integrin inhibition stained for pS660-PKCβII and Podxl. Yellow arrowheads, luminal; arrows, BL, white arrowheads, vesicular. Right panels: higher magnification of split color images from boxed regions.

(I and J) β1-integrin, PKCβII (pS660, pT641, total [anti-GFP]) and GAPDH from total cell lysates of parental (MDCK) or GFP-PKCβII-expressing cysts and either (I) scramble or β1-integrin shRNA, or (J) co-overexpressing β1A-integrin (WT, V737N). See also Figures S4 and S5 and Movies S2 and S3.

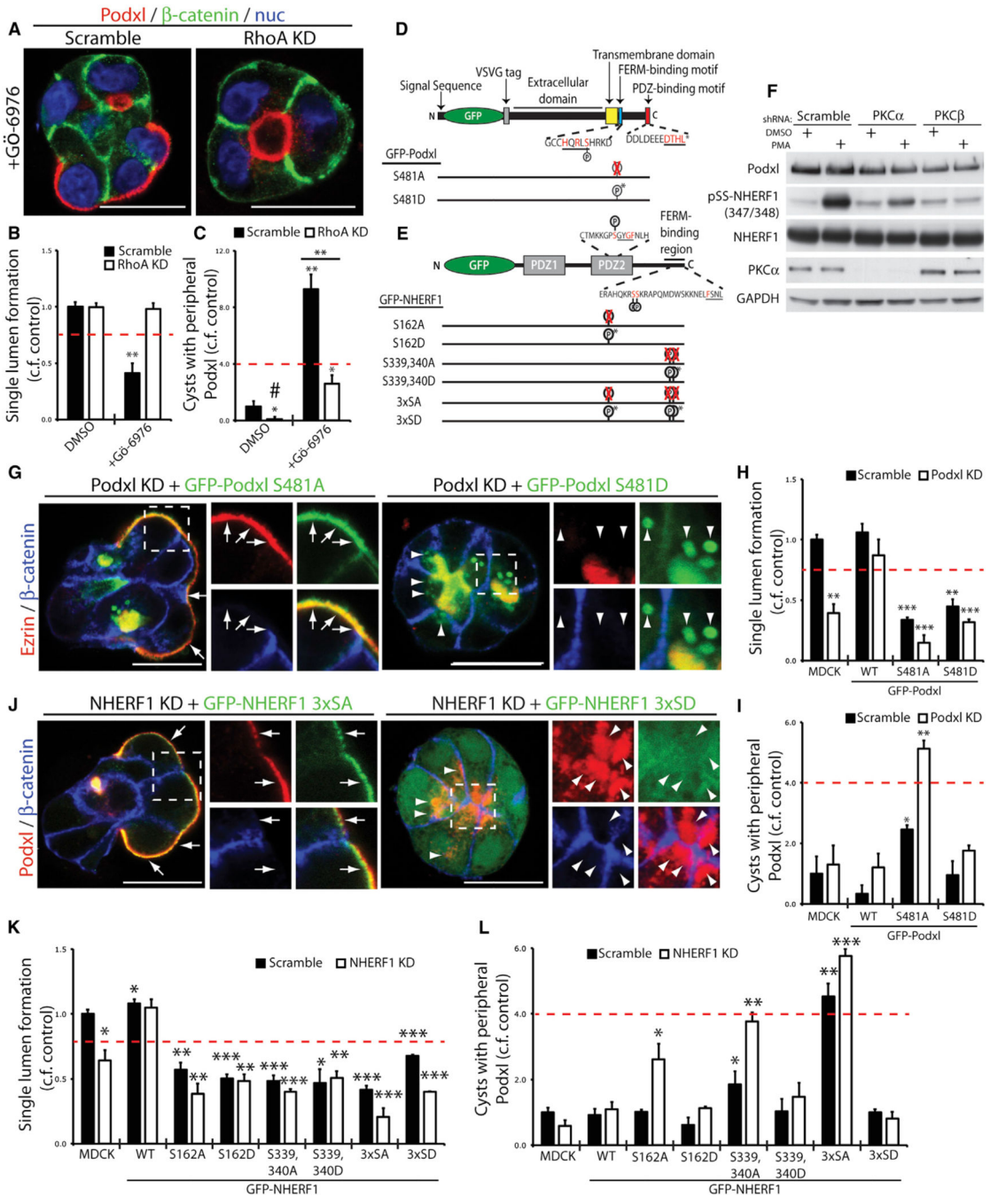

Figure 6. Podxl Complex Phosphorylation Regulates the Switch between Front-Rear and AP-BL AP Polarization

(A) Cysts expressing either control or RhoA KD grown in the presence of classical PKC inhibitor (+Gö-6976, 0.5 μM) stained for Podxl, β-catenin, and nuclei.

(B and C) Quantitation of SLF (B) or peripheral Podxl (C) in control cysts (scramble, black bars) or upon classical PKC inhibition (+Gö-6976, 0.5 μM), and with or without RhoA KD (white bars) (mean ± SD, n ≥ 100 cysts/condition/experiment, three independent experiments).

(D and E) Cartoons of GFP-Podxl (D) and GFP-NHERF1 (E) phosphorylation mutants used in subsequent experiments. 3×SA/SD, triple Ser-to-Ala/Asp mutants.

(F) Podxl, ppS347/348-NHERF1, total NHERF1, PKCα, and GAPDH expression from total cell lysates of cells expressing scramble, PKCα or PKCβ shRNAs that were serum-starved overnight, and treated with either DMSO or PMA (100 nM) for 30 min.

(G) Cysts coexpressing Podxl shRNAs and RNAi-resistant GFP-Podxl FBM phosphorylation site mutants (S481A/D) stained for Ezrin and β-catenin. Arrows, AP; arrowheads, vesicular. Smaller panels are higher magnification of split color images from boxed regions.

(H and I) Quantitation of SLF (H) or peripheral Podxl (I) in cysts upon control (scramble, black bars) or Podxl (white bars) KD without or with RNAi-resistant GFP-Podxl (WT or PKC phosphorylation mutant) coexpression (mean ± SD, n ≥ 100 cysts/condition/ experiment, three independent experiments).

(J) Cysts coexpressing NHERF1 KD and RNAi-resistant GFP-NHERF1 PKC phosphorylation-site mutants stained for Podxl and β-catenin. Arrows, AP; arrowheads, vesicular.

(K and L) Quantitation of SLF (K) or peripheral Podxl (L) in cysts upon control (scramble, black bars) or NHERF1 (white bars) KD without or with RNAi-resistant GFP-NHERF1 (WT or PKC phosphorylation mutant) coexpression (mean ± SD, n ≥ 100 cysts/condition/ experiment, three independent experiments). See also Figure S6.

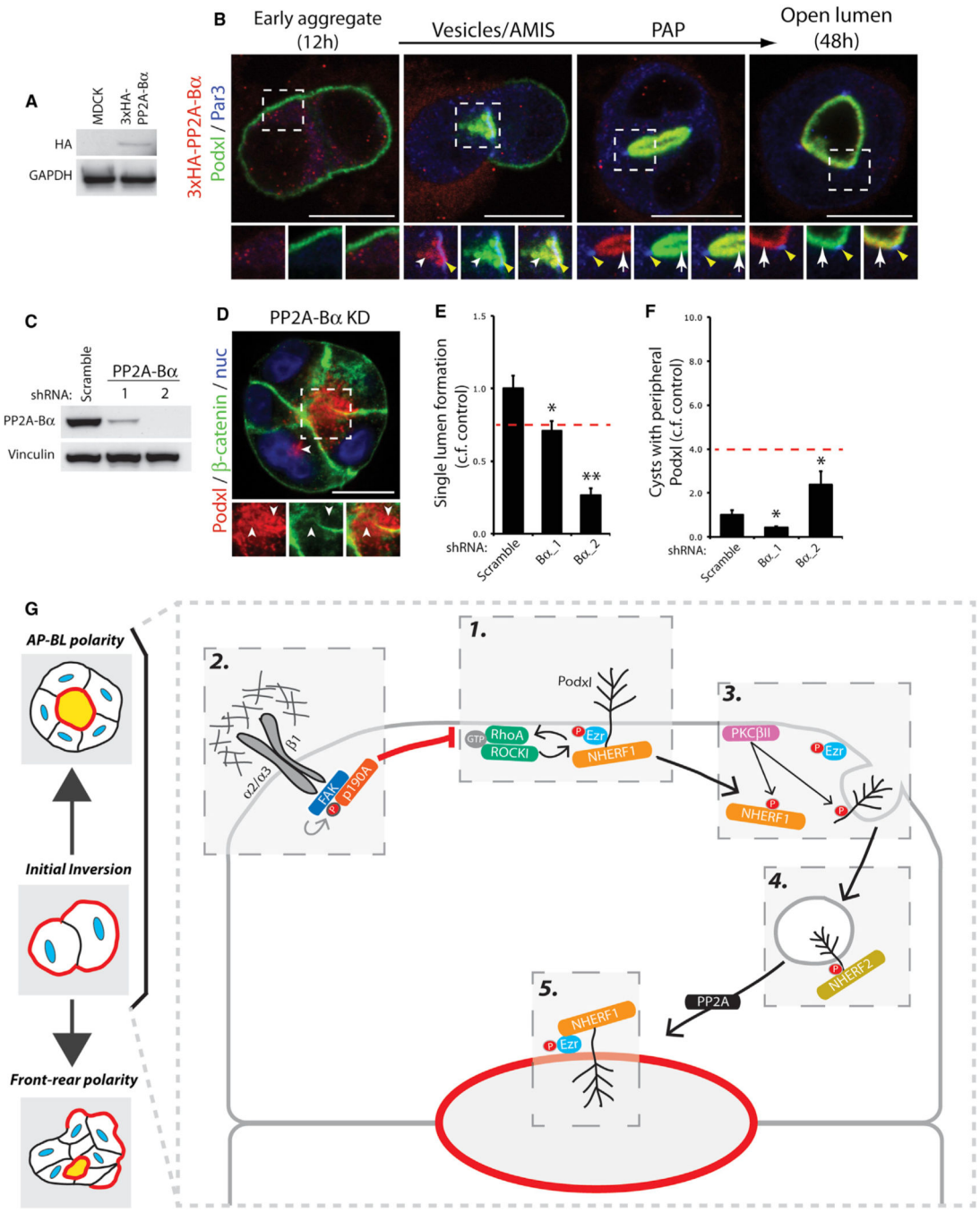

Figure 7. PP2A Controls AP-BL Polarization and Model of Polarity Orientation

(A) HA and GAPDH expression from total cell lysates of parental (MDCK) or 3×HA-tagged PP2A-Bα-expressing MDCK.

(B) HA, Podxl, and Par3 expression in 3×HA-PP2A-Bα MDCK cells during lumen formation (12–48 hr). White arrowheads, vesicular; arrows, AP; yellow arrowheads, Par3 at AMIS and tight junctions.

(C) PP2A-Bα and vinculin expression from total cell lysates of upon scramble or two different PP2A-Bα shRNAs.

(D) Cysts expressing PP2A-Bα KD stained for Podxl, β-catenin and nuclei. Arrowheads, vesicular.

(E and F) Quantitation of SLF (E) or peripheral Podxl (F) in cysts upon control (scramble) or PP2A-Bα KD (mean ± SD, n≥100 cysts/condition/experiment, three independent experiments).

(G) Model of interactions that control AP-BL versus front-rear polarization: (1) the Podxl-NHERF1-pEzrin complex is stabilized at the cell periphery via a feedback loop between RhoA-ROCKI-Ezrin, (2) an α2/α3/β1-integrin/FAK/p190ARhoGAP module breaks this feedback loop by downregulating RhoA-GTP at the periphery, (3) PKCβII phosphorylates and dissociates the Podxl-NHERF1-Ezrin complex, triggering peripheral Podxl endocytosis, (4) Podxl and NHERF2 transcytose to the AMIS, and (5) AP polarity is reestablished at the AMIS, dependent on PP2A and the reassociation of the Podxl-NHERF1-Ezrin complex.